MRTD: to NUC or not to NUC?

van Rheenen, Arthur, Thomassen, Jan

Arthur D. van Rheenen, Jan B. Thomassen, "MRTD: to NUC or not to NUC?," Proc. SPIE 11536, Target and Background Signatures VI, 115360G (21 September 2020); doi: 10.1117/12.2574691

SPIE.

Event: SPIE Security + Defence, 2020, Online Only

MRTD – to NUC or not to NUC

Arthur D. van Rheenen[1a], Jan B. Thomassen[a]
[a]Norwegian Defence Research Establishment, P. O. Box 25, N-2027 Kjeller, Norway

ABSTRACT

We applied a simple method to estimate the Minimum Resolvable Temperature Difference (MRTD) of an LWIR and an MWIR camera. A so-called Siemens star, in our case a thin, black aluminum plate framing a circle that is missing (cut out) every other spoke, is mounted in front of a black body whose temperature is relatively close to room temperature. From short recordings of the black body and Siemens star both the Noise Equivalent Temperature Difference (NETD) and the Modulation Transfer Function (MTF) are extracted and a simple estimate of MRTD = NETD/MTF is obtained. The imaged Siemens star almost completely covers the focal plane array; hence, an MRTD curve for the whole array is obtained. We investigated the effect of Non-Uniformity Correction (NUC) and Bad-Pixel Removal (BPX), two often applied pre-processing techniques, on the MRTD estimate. We find that (1) BPX has only limited effect on the result; (2) NUC is required to obtain a good MTF; and (3) NUC is not a prerequisite to obtain a good NETD estimate, but this is contingent on having a proper segmentation tool or template available. Without a segmentation algorithm, NUC together with simple intensity thresholding provides a sufficiently good segmentation and accordingly a good estimate of NETD.

Keywords: MRTD, NETD, MTF, NUC, bad pixel removal

1. INTRODUCTION

Both contrast and spatial resolution are important when trying to ascertain what target one is looking at. With a good sensor, i. e. one that has good sensitivity and high spatial resolution, the contrast between the target and the background appears to be large and a good deal of target detail can be resolved, allowing for early (at large range) identification of the target. Minimum Resolvable Temperature Difference is a function that relates the contrast, for IR sensors in terms of a temperature difference, to the spatial resolution of the sensor, expressed as number of cycles per unit of spatial angle (cy/mrad). In essence, the MRTD curve divides the space spanned by the contrast and spatial resolution parameters into "good" and "bad" half-planes. When operating above the curve, the sensor provides good contrast and spatial resolution. Below the curve, contrast and/or spatial resolution are not sufficient to for instance, identify a target at a given range. Measuring the MRTD in the lab allows one to estimate the range at which a given target may be detected or identified.

Traditionally, measurement of the MRTD is based on one or many observers studying images of, for instance, a bar pattern with different contrast and different size (spatial resolution). When an observer cannot distinguish the pattern from the background, for a given contrast and pattern size (or spatial resolution), the contrast is marked as the minimum resolvable contrast (temperature difference in IR) for that spatial resolution value. By repeating this exercise for different pattern size, a curve is built: the Minimum Resolvable Contrast or Minimum Resolvable Temperature Difference curve.

In many approaches, only a small part of the focal plane array is used to image the pattern. As a result, the obtained MRTD is strictly valid only for the part of the array that was used, not the whole array. Responsivity and noise characteristics vary over the array, even after applying Non-Uniformity Correction (NUC). With the approach we use here, we almost cover the whole array. Our aim is to obtain a single MRTD curve for the whole array.

The use of human observers in the MRTD measurement technique makes it both time consuming and costly. Modelling of the MRTD, based on easily obtainable sensor characteristics, is a way to avoid these costs. However, to obtain the same MRTD curve as from measurements, the behavior of the human eye must be modelled, since observers look at the images and are part of the measurement chain. NV-IPM[1] and TRM4[2] are examples of tools used to obtain MRTD curves and estimate target task performance measures such as detection ranges and identification ranges.

[1] arthur-d.vanrheenen@ffi.no

Target and Background Signatures VI, edited by Karin U. Stein, Ric Schleijpen,
Proc. of SPIE Vol. 11536, 115360G · © 2020 SPIE · CCC
code: 0277-786X/20/$21 · doi: 10.1117/12.2574691

In this work, we use a simple technique to obtain the MRTD, one that avoids the human observer all together. In autonomous systems, there is no human involvement and an MRTD curve obtained without the involvement of human observers is better suited to predict target task performance of said systems. The technique presented here involves making recordings of a Siemens star and estimating the Noise Equivalent Temperature Difference (NETD) and the Modulation Transfer Function (MTF) from these recordings and then to combine them, to find the MRTD curve.

In many camera systems, the raw images are improved by applying pre-processing routines. Two of these routines are bad-pixel removal (BPX) and non-uniformity correction (NUC). The first routine removes non-responsive pixels and the second equalizes the response of pixels, such that a uniform scene results in a uniform image. We investigate the effect that these two standard image-quality improving routines have on the MRTD curve we try to estimate.

In the next section we describe the measurement procedure, followed by a short section that briefly explains what BPX and NUC entails. Next, we describe how NETD and MTF are extracted from the recordings. In Section 5 we present the results from our analysis of the recordings together with a discussion of these results. We summarize our findings in the last section of this paper.

2. EXPERIMENTAL DETAILS

An “ordinary” Siemens star is a circle divided into an even number of pie pieces of equal size that are alternatingly painted white and black, see Fig. 1.

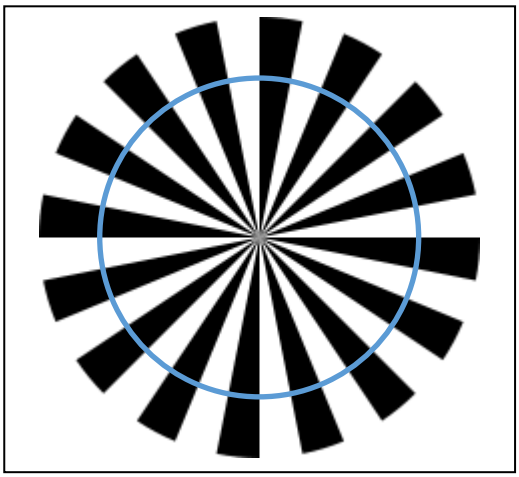

Figure 1. Example of a Siemens star consisting of 32 spokes. In our experiments, the star had twelve spokes. The circle, not a part of the Siemens star, is used to explain how the MTF is obtained, see Section 4.

In the IR version, the black pie pieces are cut out from a metal plate and the plate with the remaining pie pieces is painted black with a high-emissivity paint. This construct is reminiscent of an optical chopper, except it is not rotating. Our version consists of twelve spokes. The plate is mounted in front of a CI Systems black body, at a short distance (2 cm), and the temperature of the black body is set relatively close to room temperature. The black body emits IR radiation through the cutout pie pieces and the plate, which is at room temperature, is assumed to emit IR radiation like a black-body. Because of the temperature difference, an IR camera will perceive a contrast between alternating spokes of the star. In our experiments, the black body was set at a temperature roughly 2 K higher than room temperature. The temperature difference between the hot (black body) and cold (plate) spokes was measured with a Raytek Infrared Thermometer. We checked that the Raytek registered the same temperature as the set point of the black body over a range of temperatures about room temperature.

We made three recordings for each IR band (LW/MW005, 006, and 007) of the Siemens star mounted in front of the black body, each at a different range between the sensor and the Siemens star: 1.55, 2.96, and 6.12 m. The purpose of measuring at larger ranges is to extend the spatial frequency range of the measurements. This is explained in Section 4.

Recordings, each consisting of 200 frames taken at 100 fps, were made with an LWIR and an MWIR camera from IrCam. Camera specifics are presented in Table 1.

During the recordings, the measured black-body temperatures were 25.2, 25.1, and 25.1 ºC, whereas the temperature of the blades of the star were measured as 23.0, 23.1, and 23.5 ºC, yielding temperature differences of 2.2, 2.0, and 1.6 K, respectively.

Table 1. Specifics of the IrCam Equus327 L/SM IR-cameras used in the experiments.

Characteristic	LWIR	MWIR
Optics [mm]	50	50
F-number	2	2
Detector pitch [µm]	16	15
Focal plane (H x V) [pixels]	640 x 512	640 x 512
IFOV [µrad]	320	300
Horizontal FOV [degrees]	11.7	11.0
Spectral range [µm]	7.5 – 9.9	3.0 – 5.0
Integration time [ms]	0.1	1

3. ABOUT BPX AND NUC

We present a recapitulation of these two often-used techniques to improve how an image is perceived.

3.1 BPX

Many focal plane arrays have a small percentage (< 5%, depending on technology) of pixels that do not/poorly respond to changes in input stimulus, so called dead pixels. Often, their output value seems to be stuck at either the high or the low end of the dynamic response scale, resulting in white or black spots in the image. Sometimes this is referred to as "pepper & salt" noise. The images with their black and white spots are less pleasing to the eye and therefore they are removed during preprocessing of the images. Removal means, for instance setting their value equal to that of the mean, median, or majority value of the pixels surrounding the offending pixel. Often, camera software comes equipped with a map of the bad pixels, reducing preprocessing time. This map may be updated as camera properties change. The result of applying BPX to an image is a more pleasing viewing experience. However, it has been shown[3] that pepper & salt noise do not hinder robust image processing techniques from performing advanced target recognition. Obviously, there is a limit to how much pepper & salt noise can be tolerated, but for instance 5% of bad pixels is not a problem[3].

3.2 NUC

One would expect that a uniform object in a scene would result in a uniform (same intensity in case of IR) replica in the image. Generally, pixel response varies over the focal plane array, with some pixels responding more strongly and others more weakly to a variation in input stimulus. Most of this variability in responsivity can be ameliorated by adjusting the gain and the offset of the individual pixels in such a way that a uniform input results in a uniform response. NUC requires recordings of a uniform radiator, typically a black body, at two different temperatures to allow for a calculation of gain and offset for each pixel. Usually, the period for which the NUC holds is limited as responsivity of individual pixels drifts at different rates, but may also vary with operating conditions. Again the result of applying NUC is a much more pleasing image.

We apply NUC in the following way. The two black-body recordings are referred to as reference measurements. Each recording is averaged over a number of frames (typically 100), resulting in a single frame, which we call *ref1* and *ref2*, respectively. Let us call a single frame of the target recording *F(raw)* and the same frame after applying NUC, *F(nuc)*. Then:

$$F\left(nuc\right)=\frac{mean\left(ref\,2-ref\,1\right)}{ref\,2-ref\,1}\left(F\left(raw\right)-ref\,1\right)+mean\left(ref\,1\right) \tag{1}$$

The operator *mean* denotes averaging over all pixels in the frame.

4. ANALYSIS OF RECORDINGS: EXTRACTING NETD AND MTF

In this section, we will describe how we estimate the NETD and the MTF curve form our IR recordings.

4.1 Finding NETD

The most common approach to finding the NETD for a sensor is to record the response of the sensor to a black body operating at two different temperatures, T_1 and T_2, each recording consisting of a number (M) of frames. The signal difference $S_1(k) - S_2(k)$ for each pixel k is defined as the difference between the averages, over all frames, of the responses to the two black body temperatures.

$$S_{1,2}\left(k\right)=\frac{1}{M}\sum_{frame=1}^{M}S_{1,2}\left(k,\,frame\right) \tag{2}$$

The responsivity $R(k)$ of pixel k is defined as the ratio of the signal difference and the temperature difference:

$$R\left(k\right)=\frac{S_1\left(k\right)-S_2\left(k\right)}{T_1-T_2} \tag{3}$$

The noise $N_{1,2}(k)$ is defined for each pixel as the standard deviation of the signal strength over the frames. Often the two noise numbers are squared, summed, and taken the square-root of to obtain $N(k)$. Sometimes, the lower of the two is chosen to get a lower NETD value. Finally, $NETD(k)$ is defined as the ratio of the noise $N(k)$ and the responsivity $R(k)$:

$$NETD\left(k\right)=\frac{N\left(k\right)}{R\left(k\right)}=N\left(k\right)\frac{T_1-T_2}{S_1\left(k\right)-S_2\left(k\right)} \tag{4}$$

These values, $NETD(k)$ are then presented in the form of a histogram or averaged over all the pixels in the focal plane array to obtain the NETD value. Dead pixels or ones with a poor response could affect the average value; hence, the median value may be a better indicator of typical pixel performance.

Our approach to calculating the NETD differs from the more typical one sketched above. Rather than making separate recordings of the black body, we opted for using the same recording to extract both the NETD and the MTF. The pixels in the recorded images are already divided into two groups: hot and cold pixels corresponding to the black body and the plate in front of it. Instead of calculating the individual pixel responsivities and noise, we calculate global response and noise. To calculate the responsivity, we average the response of the hot pixels, subtract the average of the cold pixels, and then divide by the temperature difference. We calculate the noise by averaging over all pixels, the standard deviation of individual frame-to-frame (200 frames) signal fluctuations. Finally, we use the expression in Eq. (4) to calculate the NETD.

4.2 Extracting MTF

Going around the circle in Fig. 1 and registering the response of the pixels on that circle, we observe that the strength of the response changes periodically: 32 times as the phase angle increases from 0 to 2π radians. For a large circle radius, when there are a large number of pixels in each section (pie piece) the response as a function of phase angle is well approximated by a square wave, oscillating between maximum S_{max} and minimum S_{min} signal strength. At the section

edges, there may be a few pixels that have signal strengths between these two extreme values, a limitation in edge sharpness caused by several factors, amongst them the diffraction limit. As the radius of the circle is reduced, these edge effects start to become more important and the smallest signal strength on the smaller-radius circle is larger than S_{min}. Similarly, the largest signal strength will be less S_{max}. Hence, the modulation depth along the smaller-radius circle is less than value along the larger-radius circle. When we plot the modulation depth along a circle it is initially constant for large radii, but starts to drop as the circle radius becomes smaller and smaller. The inverse of the radius is proportional to the spatial frequency. This approach allows us to construct the Modulation Transfer Function, MTF.

To characterize the modulation depth for each circle radius we opt to make use of the fact that we know how many periods (six) the modulation signal has. After Fourier transform of the modulation signal as a function of phase angle, we simply pick out the sixth frequency component – its strength is a measure for the modulation depth. We normalize these signal strengths dividing them by the signal strength at low spatial frequency (large radius).

What remains is the conversion of the circle radius to a spatial frequency. We realize that the target consists of twelve segments or six segment pairs, each pair the equivalent of one cycle. The spatial frequency ν is defined as (6 cycles) / ($2\pi r$), where $2\pi r$ is the circumference of the circle with radius r. In the object plane, the radius is measured in terms of the actual size of the target. In the image plane, the radius is defined in terms of number of pixels, N_{pix}. Each pixel covers solid angle IFOV radians. With this in mind, the spatial frequency is defined as follows:

$$\nu = \frac{6}{2\pi N_{pix} IFOV}\left[cycles / rad\right] \tag{5}$$

For the smallest range (1.55 m) the circle radii range from 6 to 200 pixels. This corresponds to a spatial frequency range of 0.015 – 0.50 cy/mrad for the LW camera. The Nyquist frequency is 1/(2 *IFOV*) = 1.56 cy/mrad. This frequency limit is easily reached for the longest range (~6 m) between camera and Siemens star. The IFOV for the MW camera is 6% smaller, so the numbers are slightly different: its Nyquist frequency is 1.67 cy/mrad, but also that limit is reached when the range is 6 m.

5. RESULTS AND DISCUSSION

5.1 MTF

In Fig. 2 we give an impression of what a recording looks like (left), also in close up (right). In this case, both BPX and NUC have been applied in the pre-processing step, resulting in "clean" images.

Figure 2. Example of a recording (here LW) of the Siemens star (left) and a zoomed-in version (right) to show details about the center of the recording. The cross hairs indicate where the center of the star is. In this case, the minimum circle radius is 6 pixels and this corresponds to the highest spatial frequency that can be considered in his recording.

Figure 3 shows how analysis progresses from defining the circles of different radius in the image (top, left), to tracing the modulation signal along the circumference of the circles (top, right), to FFT results (bottom, left), and finally to an un-normalized MTF (bottom, right). We observe that the modulation signal strength is reduced when the frequency

increases. This may be not so apparent from the top-right graph, where all trace signals are plotted in one graph, similarly for the graph with the FFT's, but it is clear in the raw MTF plot. In the FFT plot the sixth frequency component sticks out (as well as its 3rd and 5th harmonics). Each of the data point (circles) in the MTF plot corresponds to a circle drawn in the original recording. This procedure is repeated for all the frames (200) in the recording: each resulting in an MTF curve. We average these MTF curves and normalize the average by dividing by the low-frequency limit value.

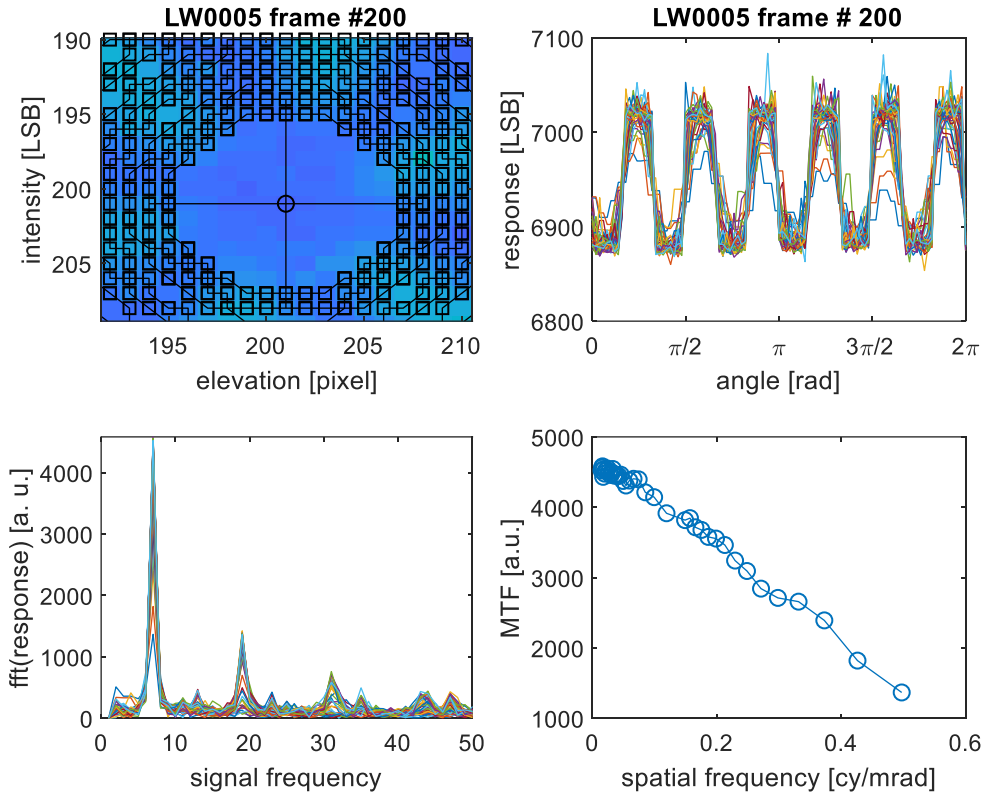

Figure 3. One frame of a recording with analysis-circles drawn in (top, left), modulation signals along these circles (top, right), FFT of modulation signals (bottom, left), raw (not normalized) MTF (bottom, right).

The effect of the two pre-processing steps on the raw image is presented in Fig. 4 and the resulting MTF curves in Fig. 5. The effect of applying NUC is clear, resulting in strongly improved MTF curves. The effect of BPX is less strong, but still noticeable. We conclude therefore, that it is essential to perform NUC to the raw images before attempting to find the MTF using the procedure described above. It also helps to apply BPX as a pre-processing step: a better MTF is obtained. These observations are not unique to this particular example, LW005, but are also made for the other recordings.. The six MTF curves (after both BPX and NUC are applied) are shown in Fig. 6. There is reasonable agreement between the three curves for each wave band, although the curve for LW005 shows a tendency towards a more limited bandwidth.

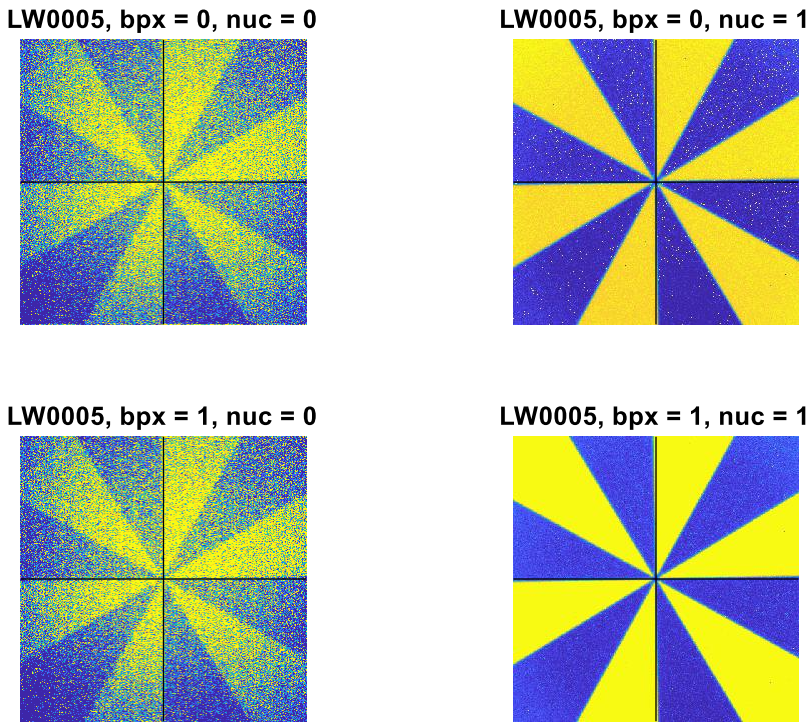

Figure 4. Effect of the pre-processing steps on the raw image. Top-left: raw image; top-right: only NUC applied; bottom-left: only BPX applied; bottom-right: both BPX and NUC applied.

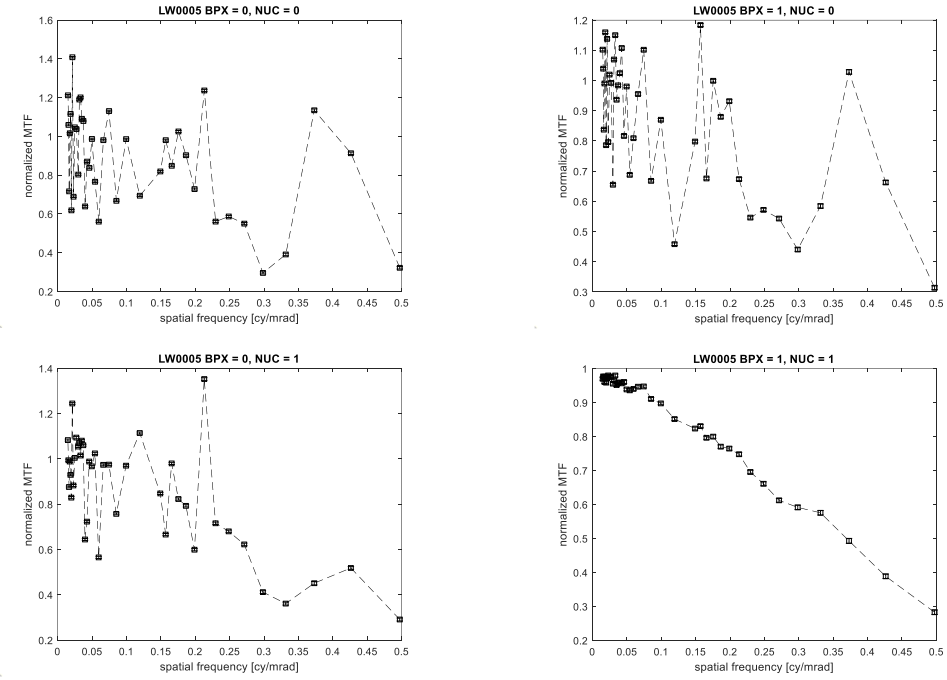

Figure 5. Effect of the pre-processing procedures on the MTF. The plots correspond to the images in Fig. 4.

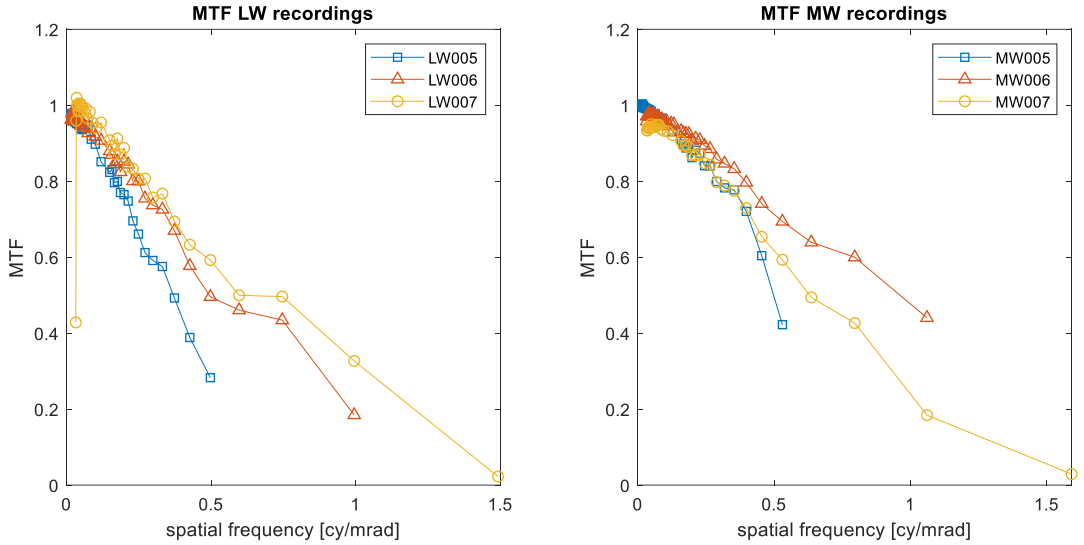

Figure 6. MTF curves obtained from the six recordings. Before extracting the MTF curves, both BPX and NUC were applied to the raw image sequences.

5.2 NETD

Partitioning the pixels in the images according to their intensity seems an appropriate approach when NUC has been applied to the images. In Fig. 4, right-hand column, there seems to be a clear spatial distinction between the hot (yellow) and cold (blue) pixels. Clearly, this is much fuzzier when we do not apply NUC (see left-hand column in Fig. 4). Here, "yellow" pixels appear in the "blue" fields and vice versa. The correlation between pixel intensity and spatial location is much weaker.

To be able to make a fair comparison we chose to use the NUC'ed image to divide the pixels into hot and cold pixels and use this identification of location to partition the pixels in the raw image as well. We illustrate this in Fig. 7.

For each frame of the recording, we calculate the median pixel intensity (med) and the mean absolute difference (mad). Pixels are divided into two groups: those that have intensity less than $med - 0.1 \cdot mad$ and those that have intensity larger than $med + 0.1 \cdot m$.

In Fig. 7 we show the histograms of the cold (blue) and hot (orange) pixels in a raw frame, at the top. The pixel intensities are partitioned by determining whether their value was lower (cold) than the median value or higher (hot). In the bottom histogram, the pixels in the NUC-and-BPX-applied frame are partitioned according to their median value. When we apply the latter partition to the raw frame, we obtain the histogram in the middle of the figure.

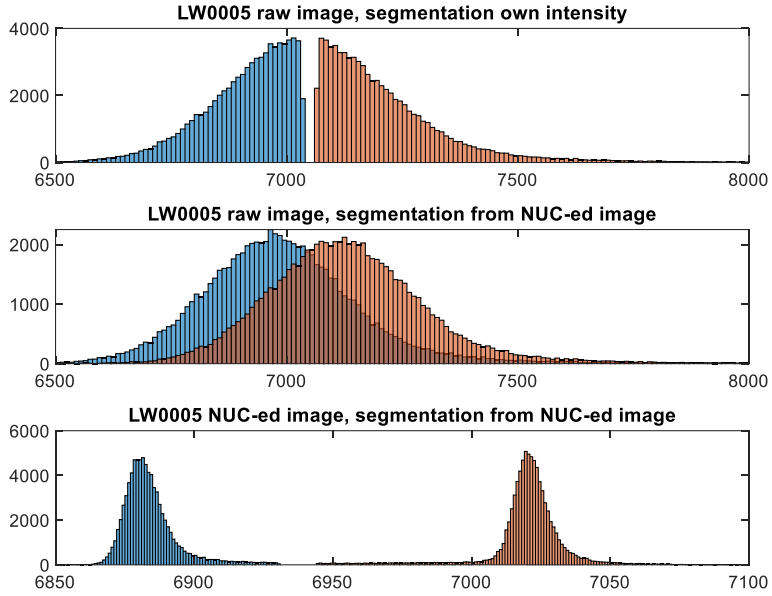

Figure 7. Histograms of cold (blue) and hot (orange) pixel intensities: raw image, partition based dividing intensities into larger than and smaller than median intensity (top), image where NUC was applied (bottom), and partition from the NUC-applied image used in the raw image (middle).

When we apply this procedure, determining the grouping of the pixels from the NUC-and-BPX-applied frame, where we assume there is a strong intensity–spatial location correlation, to the other frames that were or were not exposed to the pre-processing procedure, we obtain the NETD values listed in Table 2.

Table 2. NETD values [mK] based on grouping obtained from the fully pre-processed image (both BPX and NUC applied)

Recording	Raw	NUC only	BPX only	NUC and BPX applied
LW005	58	58	57	57
LW006	36	55	36	56
LW007	31	46	31	46
MW005	58	58	55	54
MW006	52	57	50	55
MW007	48	51	47	49

5.3 Masking excess pixels

For LW005 and MW005 there seems to be little effect of applying NUC as a pre-processing step, as long as the frames are correctly segmented into the cold and hot regions. Applying BPX has a small effect. For the other recordings, applying NUC results in higher NETD values, and seems to be detrimental to a good estimate of sensor performance: the lower NETD values must be better. However, the NETD values come about by dividing the noise of the pixels by their responsivity. We show that the lower NETD values are an artifact of the method of grouping the pixels. Using the median pixel intensity as a separating criterion requires that there are roughly as many hot as cold pixels. The cropped images are squares, enclosing the Siemens star, which is essentially a circle. With the Siemens star in the middle of the frame, the corners are outside the circle and that means that there are a good many more cold pixels than hot ones, skewing the median intensity value towards the cold distribution. This effect can be countered by applying a circular mask and ignoring all the pixels outside the circle. This guarantees equal numbers of hot and cold pixels. In Table 3, we show the NETD values that we obtained after applying the mask.

Table 3. NETD values [mK] based on grouping obtained from the fully pre-processed image (both BPX and NUC applied) and after rejecting all pixels outside a circular mask.

Recording	Raw	NUC only	BPX only	NUC and BPX applied
LW005	55	57	55	57
LW006	51	53	51	53
LW007	40	42	40	42
MW005	57	57	54	54
MW006	56	56	52	53
MW007	50	50	48	48

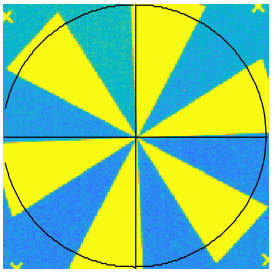

Inspecting the entries in Table 3, we observe that the pre-processing steps BPX and NUC have only small effect on NETD. If anything, NUC slightly (~2 mK) worsens NETD in the LW recordings and BPX seems to provide a small improvement (~ 2-4 mK) in the MW recordings. Provided, the images are properly segmented into hot and cold regions, pre-processing has a marginal effect on estimating NETD.

5.4 Alternative approach to estimate NETD

As a check to see whether we arrived at correct NETD values, we looked at the pixels inside a box that straddles a hot-cold transition. In Fig. 8, we show two versions of the frame under consideration, with boxes drawn in (top row in Fig. 7). For each box, pixel intensities are averaged along the transition and then profiles across the transitions are plotted (bottom row in Fig. 8).

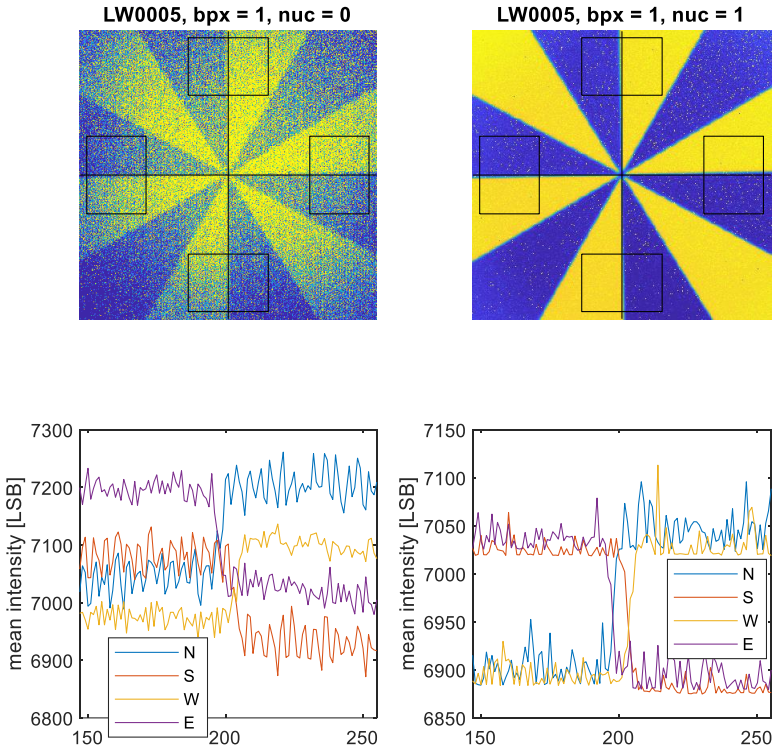

Figure 8. Frames with boxes (top row) and average response curves across the hot-cold transition for all four boxes. The labels N, S, W, E refer to the location (North, South, West, East) of the boxes in the frames

The labeling N, S, W, E refers to the location of the boxes in the image. The contrast is estimated from these curves by calculating the difference between the average signal levels away from the transition. Now, the average responsivity of the pixels inside the box can be calculated. The pixel noise is calculated as described earlier. In this approach, we are guaranteed that pixels on either side of the transition are appropriately assigned to the hot and cold groups, respectively. Obviously, this is only a local check, we do not use the whole image, but averaging over the four boxes may give a good indication of the correct NETD values.

The response curves for the image where NUC was applied clearly are better aligned and show smaller fluctuations, but the average contrast is barely affected. The resulting NETD values for this analysis are presented in Table 4.

Table 4. NETD [mK] values for the four boxes in Fig. 7, as well as the other pre-processed frames.

LW005 NETD	North	South	West	East	Mean
Raw	50	53	69	47	54.4
NUC only	54	53	59	54	54.9
BPX only	51	54	67	46	54.4
NUC & BPX	54	53	59	54	54.9

Although there is some spread in the NETD values from box to box, i.e. across the focal plane array, the mean values vary very little: from 54.4 to 54.9 mK. Apparently, the pre-processing does not affect the estimation of NETD. In Table 5, we present average values for the other recordings.

Table 5. Averaged, over four areas in the focal plane, NETD values derived from analysis of intensity profiles across a hot-cold transition (see Fig. 7)

Mean NETD	LW005	LW006	LW007	MW005	MW006	MW007
Raw	54.4	50.4	40.1	54.3	49.4	47.5
NUC	54.9	51.6	40.4	55.4	50.3	48.0
BPX	54.4	50.3	39.2	54.7	49.7	46.9
NUC & BPX	54.9	51.6	40.4	55.4	50.3	48.0

Table 5 shows us that pre-processing only marginally affects the estimates of NETD that we obtain. It also shows that the values are aligned with those obtained above (Table 3). In addition, we identify the same trend of lower NETD values from LW005 to LW007 and from MW005 to MW007. The difference between the recordings is that they are made of the same object, but at increasing ranges. This implies that a smaller part of the focal plane array is used to image the Siemens star. Whereas in the shortest range recordings more of the off-center pixels are used, in the longest range recordings only the center pixels are used to image the star. Possibly, the performance of the focal plane array is best in the center of the array (both in LW and MW), also when NUC and BPX are applied. The noisiness of the pixels does not change very much, but the average responsivity ($\Delta S/\Delta T$) increases both in LW and MW, from recording 005 to 007.

5.5 MRTD

The final step in the analysis is to divide the NETD by the MTF. We present the results in Fig. 9. We include MRTD curves that we obtained during an observer trial, performed in 2016, where an observer was asked to report how many of the six bar pattern of different size he could discern in the recorded imagery when the contrast was reduced. The observer was allowed to adjust gain and offset when viewing the imagery. The same sensors were used during the observer trial and the experiments described here, however, at that time a 200-mm lens was used rather than a 50 mm lens. We adjusted the frequency scale of the observer data by dividing by four. Machine analysis of the recordings made during the observer trial produced similar results[4]. The observer trial seems to produce lower values for the low-

frequency limit of the MRTD curves than what the current analysis yields, especially for the MW band. In this case, the observer trial yielded an unrealistically low NETD value, even. We mention that the "room temperature" during the observer trial was significantly higher and a different lens was used at that time. Other than this discrepancy, we observe roughly the same behavior.

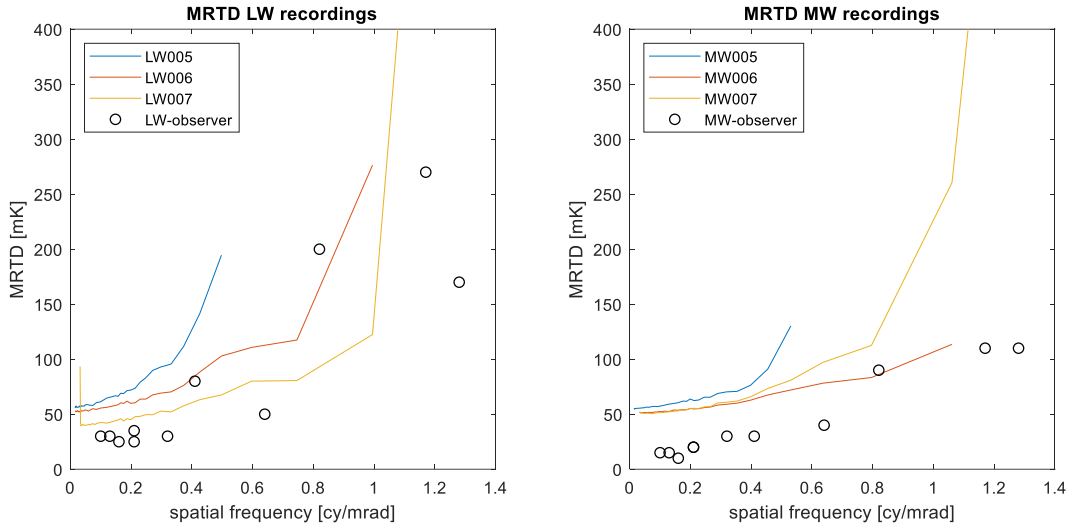

Figure 9. MRTD curves obtained from the three LW recordings (left panel) and the three MW recordings (right panel): the solid lines indicate them. An earlier observer trial using the same sensors also produced MRTD data[4]: these are the black circles.

6. SUMMARY

We used IR recordings of a Siemens star to estimate an important sensor-performance characteristic, the MRTD curve, which relates sensitivity to spatial resolution. This characteristic plays a decisive role in the process of estimating range performance of IR sensors. We model the MRTD in its simplest form as the ratio of the NETD and MTF. The latter two quantities are individually extracted from the recordings. There are several reasons for attempting to find the MRTD this way: (1) we like to avoid costly observer trials, (2) we like to obtain an MRTD that is representative of the entire focal plane array, and (3) we like to avoid having to be dependent on pre-processing the raw imagery if possible. In other words, we like to use the simplest of procedures to obtain this important characteristic.

The MTF is found by logging the intensity profile along circles with decreasing radius about the center of the imaged star. The spatial frequency is inversely proportional to the circle radius and the modulation depth is proportional to the strength of the N'th frequency component of the FFT of the intensity profile, where N is the number of pairs of black and white spoke pairs in the star. We found that not applying any pre-processing to the raw imagery resulted in unintelligible MTF curves. We limited the pre-processing to two procedures, BPX and NUC, and studied how they effected the estimation of the MTF curves. We conclude that it is essential to apply NUC before attempting to extract the MTF in the way we propose here, and that BPX certainly smooths the curves. In short, NUC is necessary and BPX is desirable to obtain good MTF curves. The MTF curves vary a bit from recording to recording. We have no explanation for this, other than suggesting that focus may play a role: the focus may vary over the focal plane array.

We showed that it is possible to obtain good NETD data from the recordings without applying any pre-processing at all. Finding the NETD is a two-step process, involving finding the noisiness of the pixels and their responsivity. The former is obtained by calculating the standard deviation of each pixel intensity variation over the length of the recording. The latter requires, and here we deviate from classical ways of estimating NETD, finding the mean contrast between the two groups of pixels that make up the two spokes in the image. Rather than looking for the response of individual pixels to

different input signals (temperatures, here), we look for the contrast (response) between groups of spatially separated pixels. This requires a segmentation. Without applying more advanced signal processing, this may be a challenge when no pre-processing is applied. A simple attempt at segmentation, based on intensity thresholding, fails dramatically, as we showed. The raw image simply has too many cold pixels in the hot segments of the star and too many hot pixels in the cold segments. We showed that applying NUC allows for a sufficiently good segmentation based on simple thresholding. We verified these results by locally (in the image) checking the response across a hot-cold transition and concluded that we obtained the same NETD values. During this last check, we also found that pre-processing was not required to obtain the NETD values, but that of course assumed that the images were already segmented correctly.

There is a tiny, but consistent, detrimental effect of NUC on NETD. Looking at Table 5 we observe that the NETD value after NUC is applied is always larger than without, even though this is only a fraction of one mK. Although the NUCing is a linear process in itself. NUCing consists of translating pixel intensities by individual amounts, multiply by individual gains and translating back by a fixed amount, it is not a given that a pixel that lies of the left flank of the raw intensity distribution ends up on the same flank after NUC is applied. The initial individual translations and the individual gains form a distribution of values, and it is not a given that the convolution of the distributions maintains the original ordering of pixel intensities. Hence, it should not come as a surprise if NUC affects the NETD. Apparently, the net effect is small.

A stronger effect we observe is that as at larger range a smaller fraction in the center of the focal plane array is used to image the Siemens Star, the NETD value is reduced. We observe this in both the LW and the MW band. Possibly, performance is better in the center of the arrays than out at the edges. Since NUC is based on global averages, i. e. involving averages over the entire focal plane array, this does not apparently equalize performance.

We observe that there is a spread in the obtained MRTD curves. This is caused by both differences in NETD, which scales the MTF curves, and the MTF curves themselves. Earlier measurements of MRTD, based on an observer trial, produced results that are compatible in the case of LW but markedly lower than curves obtained here, in case of MW. Those earlier measurements produced an unrealistically small NETD value. Scaling with NETD values obtained in this study provides a better match.

To answer the question in the title: it is necessary to apply NUC to the raw images in order to obtain good MRTD curves. This is entirely because it is impossible, for the approach used here, to find MTF curves without applying NUC. NETD may be determined without applying NUC, but this is contingent on having a sufficiently good segmentation algorithm or a priori knowledge of where the cold and hot pixels are physically located in the image plane. With the known target, one could have designed a template to group pixels. Otherwise, when NUC is applied, NETD can be estimated without any further segmentation or use of a template.

REFERENCES

[1] NV-IPM, < https://c5isr.ccdc.army.mil/inside_c5isr_center/nvesd/integrated_performance_model/> (24 august 2020)

[2] TRM4, < https://www.iosb.fraunhofer.de/servlet/is/44119/> (24 august 2020)

[3] Palm, H. “Fast and robust image processing algorithms based on approximations to order statistics”, Proc. SPIE 10648 (2019).

[4] van Rheenen, A. D., Taule P., Thomassen, J. B, and Madsen, E. B.,”MRTD - Man vs. Machine”, Proc. SPIE 10625 (2018).